Published July, 2001

State Space Analysis of Soil Water and Salinity Regimes in a Loam Soil Underlain by Shallow Groundwater

L. Wu,* T. H. Skaggs, P. J. Shouse, and J. E. Ayars

ABSTRACT

Improved methods of irrigation scheduling are needed to reduce irrigation and drainage water volumes while not affecting yield. State space models based on mass balance principles and empirical flux laws can be used to estimate and forecast soil water and salinity regimes in the field. In this research, a state space model was developed that describes soil water and salinity dynamics and includes the effects of shallow, saline groundwater. The model was evaluated using daily time domain reflectometry (TDR) measurements of the soil water content (θ) and bulk soil electrical conductivity (EC_b). Data were collected throughout the 1997 growing season in a field where cotton (*Gossypium hirsutum* L.) was being grown using an experimental shallow groundwater management technique that was designed to reduce both irrigation and drainage volumes. The model was tested by supposing that either weekly or biweekly profile-averaged measurements of θ and EC_b were available, and then comparing the resulting filtered model forecasts with the full data set. The results show that the measured water content was within the predicted confidence intervals of 1- or 2-wk forecasts of the profile-averaged water content, soil water EC (EC_w), and EC of saturated extract (EC_e), even though the performance of the model in predicting the resident salt concentration (mass of salt per volume of soil) was less satisfactory.

Prudent irrigation scheduling not only saves water, but also reduces the potential for non-point source pollution. Irrigation scheduling is typically based on soil or plant monitoring or evapotranspiration (ET) estimation, both of which have drawbacks. Soil or plant monitoring provides information about the current status of the soil or plant, but does not predict when future irrigation will be needed. Irrigation scheduling based on ET estimation is not site-specific, and does not take into account, for example, the salinity conditions in the field. Therefore, there is a need to develop new techniques that provide flexible irrigation schedules in real time, and that meet irrigation requirements with a minimum amount of water.

Time-series methods have been used more frequently in hydrologic investigations and water quality management during the past a few decades (Hipel et al., 1977). Using the hydrologic budget and soil water transport equations, Parlange et al. (1992) developed a first-order autoregressive Markovian model to estimate the soil water regime in the top 1.05-m soil profile. The predicted water storage in the soil profile was close to that measured by a neutron probe. Wu et al. (1997) found that changes in soil moisture could be modeled as an autoregressive-moving average process.

L. Wu, Dep. of Environmental Sciences, Univ. of California, Riverside; T.H. Skaggs and P.J. Shouse, George E. Brown, Jr. Salinity Lab., 450 W. Big Springs Rd., Riverside, CA 92507; J.E. Ayars, USDA-ARS, Water Management Research Lab., Fresno, CA 93727. Received 17 June 2000. *Corresponding author (Laowu@mail.ucr.edu).

Published in Soil Sci. Soc. Am. J. 65:1065–1074 (2001).

Aboitiz et al. (1986) used the water balance equation and reference evapotranspiration (ET_o) for an irrigated field to develop a state space model capable of estimating and forecasting soil water depletion and crop ET. Their formulation allows for real-time estimation of soil moisture and associated estimation errors. Or and Hanks (1992) developed a state space model of the soil water balance and potential ET and used Kalman filtering to obtain temporal soil water storage estimates and estimation errors. In Kalman filtering, model predictions are updated as new measurements on the system state variables become available. Or and Hanks found that the estimated soil water storage agreed better with measured values when the estimates were based a combination of spatial and temporal data, rather than on either spatial or temporal information independently. Skaggs and Mohanty (1998) developed a state space model that described shallow water table dynamics in a tile-drained field. Their formulation did not include the vadose zone water content.

The previous state space formulations of soil moisture dynamics did not consider groundwater recharge–discharge. In an irrigated soil with a shallow groundwater table, a significant amount of groundwater can be used by plants (Wallender et al., 1979; Ayars and Schoneman, 1986; Torres and Hanks, 1989). The salinity level of the root zone is also a concern for crop growth and yield. From an agricultural production standpoint, the concentration of dissolved salts in soil water, commonly quantified by the electrical conductivity of the water (EC_w), is a critical parameter. State-space models based on site-specific measurements will be able to estimate and forecast the soil water and salinity regime, which will provide flexible irrigation scheduling for farmers.

The objectives of this research were (i) to develop a state-space model for the root zone water content and salinity that includes the effects of shallow groundwater; (ii) to estimate and forecast the soil water and salinity regimes in an irrigated soil with a shallow groundwater table; (iii) to evaluate the effect of the observation interval on estimation errors associated with the Kalman filter (KF); and (iv) to evaluate the effects of upward groundwater flow on root zone salinity.

MATERIALS AND METHODS

Field Experiment

Our research site was Section 13-4 in the Broadview Water District in Firebaugh, CA. The field is a commercial farm and is approximately 60 ha. Ninety percent of the field is a Cerini series (fine-loamy, mixed, superactive, thermic Fluventic

Abbreviations: EC, electrical conductivity; ET, evapotranspiration; KF, Kalman filter; TDR, time domain reflectometry; θ, soil water content.

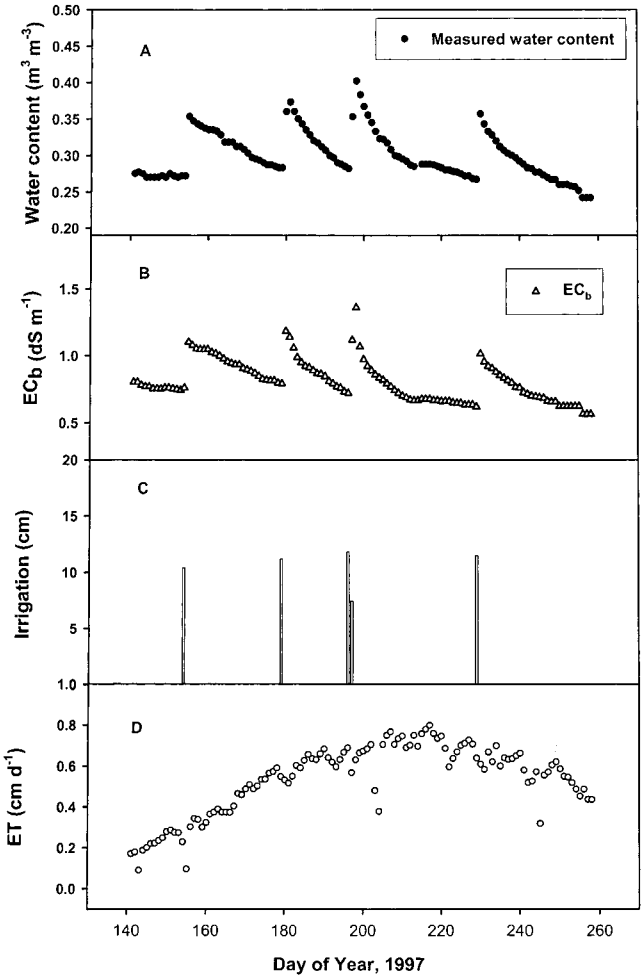

Fig. 1. (A) Field measured profile-averaged water content, $\bar{\theta}_k$, (B) bulk electrical conductivity, $\overline{EC}_b$, (C) irrigation input, and (D) estimated evapotranspiration (ET) during the growing season, 1997.

Haplocambids). Ten percent, the northwest and southeast corners, are a Tranquillity series (fine, smectitic, thermic Sodic Haploxerert).

The field contains a subsurface drainage system with drain laterals buried 1.5 to 1.8 m deep, running east–west, 123 m apart. The collector drain is located on the east side of the field. At the low end of the collector drain, we installed a device that regulates flow in the drainage system and permits control of the water table depth. The purpose of the modified drainage system is to maintain the water table at a depth that allows crops to obtain water through upward flow of groundwater, with the larger objective being a reduction in both irrigation and drainage volumes. Preliminary studies conducted over two cropping cycles found that irrigation requirements were reduced by 15 to 20% without reduced yields of tomato (*Lycopersicon esculentum* Mill.) or cotton. The efficiency of this type of shallow groundwater management will depend in part on irrigation scheduling. The long-term sustainability will be determined by the extent to which the induced upward flow of groundwater salinizes the root zone.

This study focuses on a short-term experiment conducted to evaluate plot-scale root-zone soil water and salinity dynamics over a single growing season. The field was planted to cotton during the spring of 1997, and throughout the growing season drain flow was regulated so that the water table on the east side of the field was maintained at a depth about 1.2 m. Irrigation scheduling was based on 60% allowable soil water depletion.

Three-rod TDR probes 20 cm long were installed at 10, 30, 50, 70, 90, and 110 cm below the surface at three sites along a transect perpendicular to the drainage lines in the northeast corner of the field. The three sites were approximately 70 m apart. The TDR instrumentation was used to make daily measurements of the volumetric water content and bulk soil EC (EC_b) from Day 141 (21 May) through Day 258 (15 September), 1997 (Herkelrath et al., 1991; Whalley, 1993; Schaap et al., 1996). In this paper we focus mainly on the data from Site 1.

Figures 1A and 1B show the profile-averaged (to depth 120 cm) water content, $\bar{\theta}_k$, and bulk soil EC, $\overline{EC}_{bk}$, measured at Site 1 on Days k = 141...258. These two series were constructed by averaging the daily TDR measurements over the six depths.

Furrow irrigation records kept by the farm were not sufficient to determine the timing and volume of water applied to our experimental plots. For modeling purposes, we assumed the water applied during irrigation was equal to the increase in the total water stored in the soil profile, as measured by TDR. The resulting irrigation series I_k, which is an average over the three sites, is shown in Fig. 1C. Although our analyses focus on one experimental plot, we use the averaged irrigation value because in practice irrigation amounts will be known only approximately. There was no measurable precipitation during our study.

The daily actual evapotranspiration (ET_{ak}) was calculated as

$$ET_{ak} = Kc_k ET_{ok} \quad [1]$$

where the reference ET_o was obtained from the California Irrigation Management Information System (CIMIS Station 7, Firebaugh/Telles) and the crop coefficient was calculated according to the regression equation reported in Cotton Production Manual (University of California-Division of Agriculture and Natural Resources, 1996):

$$Kc_k = 4.29 - (9.46 \times 10^{-2})k + (6.49 \times 10^{-4})k^2 - (1.29 \times 10^{-6})k^3 \quad [2]$$

where k is day of the year. The resulting ET_{ak} time series is shown in Fig. 1D.

We also monitored irrigation water, groundwater, and drainage water quality and crop yield. The irrigation water was from a reservoir and had a total dissolved salt concentration of approximately C^I = 288 mg L^{-1} with little variation over the season, whereas the groundwater had a salt concentration of approximately C^{GW} = 3840 mg L^{-1}. The ET and irrigation time series shown in Fig. 1 are used as forcing functions in our simulation model, which is described next.

State Space Modeling

State space models consist of two parts, a dynamics equation that describes the time evolution of the system state, and a measurement equation that relates system state variables to measurable quantities. The dynamics equation usually consists of a statement of mass balance and empirical flux laws that specify system fluxes in terms of state variables. Model predictions are obtained through a cycle of model forecasting and measurement updating, known as filtering. In this section we develop a state space model for root zone soil water and salinity.

Water Balance Equation

Assuming that there is no runoff and that water flow in the root zone is one dimensional, the water balance equation can be expressed as:

$$\int_0^L \frac{\partial \theta}{\partial t}\,dz = P + I - ET_a - D + R \qquad [3]$$

where P is the precipitation rate, I is the irrigation rate, ET_a is the actual evapotranspiration rate, D is the root zone drainage rate to groundwater, R is the root zone recharge rate from groundwater, θ is the volumetric water content, t is time, z is depth, and L is the depth of the root zone. Although there was no measurable precipitation in our study, we include it here for the sake of generality.

Integrating Eq. [3] with respect to time and dividing both sides by L yields the following expression for the profile-averaged water content on day $k + 1$ ($\bar{\theta}_{k+1}$):

$$\bar{\theta}_{k+1} = \bar{\theta}_k + (P_k + I_k - ETa_k - D_k + R_k)/L \qquad [4]$$

where

$$\bar{\theta}_k = \frac{1}{L}\int_0^L \theta_k dz. \qquad [5]$$

Salt Balance Equation

Assuming negligible salt uptake by plants and no precipitation or dissolution of salts, the salt balance equation can be formulated similarly to the water balance equation:

$$\int_0^L \frac{\partial \theta C}{\partial t}\,dz = PC^P + IC^I - DC^D + RC^{GW}, \qquad [6]$$

where P, I, R, and D are as defined above, C^P is the salt concentration of precipitation, C^I is the concentration of irrigation water, C^D is the concentration of drainage water, and C^{GW} is the concentration of groundwater water.

Assuming that $C^P = 0$, that C^I and C^{GW} are constant over the growing season, and that C^D is constant over a given day, integrating Eq. [6] and dividing by L yields:

$$\bar{S}_{k+1} = \bar{S}_k + (C^I I_k + C^{GW} R_k - C_k^D D_k)/L, \qquad [7]$$

where

$$\bar{S}_k = \frac{1}{L}\int_0^L \theta_k C_k\,dz \qquad [8]$$

is the profile-averaged mass of dissolved salt per unit volume of soil on day k.

State Dynamics Equation

In developing a model for the soil water and salinity dynamics, we make the following assumptions:

1. We assume the water table depth is more or less constant during the growing season, remaining at or very near the root zone depth L. Data from observation wells located near the experimental plots verified that this was a reasonable approximation during our study.
2. Defining $G_k = R_k - D_k$ as the net daily water flux at the bottom of the root zone, we assume that

$$G_k \equiv R_k - D_k = \alpha\bar{\theta}_k + \beta, \qquad [9]$$

where, for our study site,

$$\alpha(\bar{\theta}_k) = \begin{cases} -36.4\text{ cm} & \bar{\theta}_k > 0.34 \\ 0\text{ cm} & \text{Otherwise} \end{cases} \qquad [10]$$

and

$$\beta(\bar{\theta}_k) = \begin{cases} 12.5\text{ cm} & \bar{\theta}_k > 0.34 \\ 0.2\text{ cm} & \text{Otherwise} \end{cases}. \qquad [11]$$

Thus we assume the net water flux at the bottom of the root zone on a given day, G_k, is a piece-wise linear function of that day's profile-averaged water content, $\bar{\theta}_k$. Our rationale for making G_k a function of $\bar{\theta}_k$ is the supposition that when the soil is wet, drainage out of the root zone to groundwater occurs ($G_k < 0$), and when the soil is dry, upward flow from the shallow groundwater occurs ($G_k > 0$). The $G_k(\bar{\theta}_k)$ relationship specified by Eq. [9] to [11] is shown as a solid line in Fig. 2. For profile-averaged water contents less than 0.34, Eq. [9] to [11] predict $G_k = 0.2$ cm of water per day will move from the groundwater to the root zone. For $\bar{\theta}_k > 0.34$, it is predicted that G_k drops off linearly, crossing over to profile drainage ($G_k < 0$) at a water content slightly greater than 0.34. We arrived at the specific form of Eq. [9] to [11] by examining the experimental data shown as open circles in Fig. 2. These data are the "observations" of the daily net water flux at the bottom of the root zone, G_k, plotted vs. the daily measured $\bar{\theta}_k$. The "observed" G_k is calculated according to the water balance equation (Eq. [4]), $G_k = R_k - D_k = (\bar{\theta}_{k+1} - \bar{\theta}_k)L - I_k - P_k + Et_{a_k}$, using the daily data for I_k, P_k, and ETa_k that are shown in Fig. 1 and measured water content data for all three experimental plots. It is evident from Fig. 2 that both the functional form and the parameter values used in our $G_k(\bar{\theta}_k)$ model are based on subjective choices. It is also clear from the scatter of the data that the $G_k(\bar{\theta}_k)$ model is inexact. Below, we account for this imprecision by introducing a random noise term.

3. The profile-averaged salt concentration of water is approximated to be $\bar{C}_k = \bar{S}_k/\bar{\theta}_k$ (see Eq. [8]).
4. The salt concentration of water draining out of the soil profile is assumed to be equal to the profile-averaged concentration, $C_k^D = \bar{C}_k$.
5. For purposes of calculating the salt flux at the bottom of the root zone, we assume that either profile drainage or recharge occurs on a given day, but not some combination of the two. Thus, the daily salt flux at the bottom of the root zone can be approximated as $C^{GW}G_k$ when $G_k > 0$, and as $C_k^D G_k = (\bar{S}_k/\bar{\theta}_k)G_k$ when $G_k < 0$.

These assumptions and definitions for the various water and salt fluxes can be substituted into the water and salt balance equations to obtain the following (nonlinear) state equation that describes the time evolution of the state variables $\bar{\theta}_k$ and $\bar{S}_k$:

$$\begin{bmatrix} \bar{\theta}_{k+1} \\ \bar{S}_{k+1} \end{bmatrix} = \begin{bmatrix} (1 + \alpha_k/L)\bar{\theta}_k + \beta_k/L \\ \bar{S}_k + (\alpha_k\bar{\theta}_k + \beta_k)C_k^*/L \end{bmatrix} + \begin{bmatrix} 1/L & 1/L & -1/L \\ 0 & C^I/L & 0 \end{bmatrix} \begin{bmatrix} P_k \\ I_k \\ ET_{ak} \end{bmatrix} + \begin{bmatrix} w_k^\theta \\ w_k^S \end{bmatrix}, \qquad [12]$$

where $\alpha_k \equiv \alpha(\bar{\theta}_k)$, $\beta_k \equiv \beta(\bar{\theta}_k)$,

$$C_k^* = \begin{cases} \bar{S}_k/\bar{\theta}_k & G_k < 0 \\ C^{GW} & G_k \geq 0 \end{cases} \qquad [13]$$

and $\mathbf{w}_k = [w_k^\theta, w_k^S]^T$ is a random noise sequence with covariance $\mathbf{M}_k$. The first term on the right-hand side of Eq. [12] represents the internal system dynamics. The second term represents the external forcing of the system. The noise term accounts for errors introduced by the various simplifying assumptions, as well as our inability to specify exactly the forcing terms P_k, I_k, and ET_{ak}. The noise covariance is quantified below in the parameter estimation section.

State Forecasting

Equation [12] can be written more compactly as

$$\mathbf{x}_{k+1} = \mathbf{a}_k(\mathbf{x}_k) + \mathbf{B}\mathbf{u}_k + \mathbf{w}_k, \qquad [14]$$

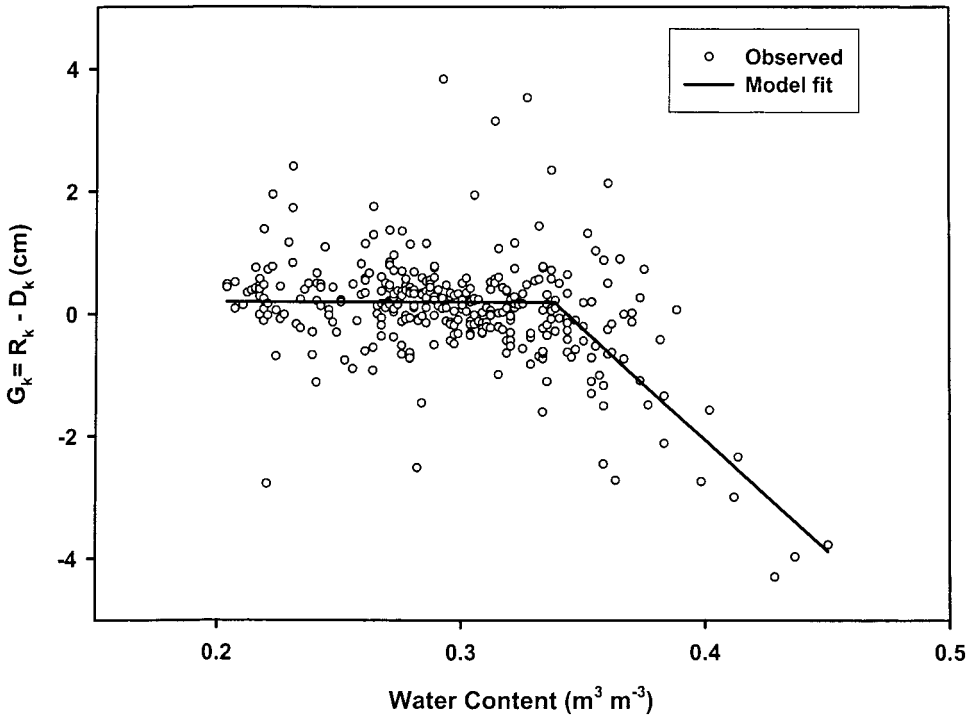

Fig. 2. Observed and regression lines of groundwater recharge (+) and discharge (−) as a function of profile-averaged soil water content.

where $\mathbf{x}_k \equiv [\overline{\theta}_k, \overline{S}_k]^T$ is the system state variable, and where lower case letters are vectors and upper case letters are matrices. The noise term in Eq. [14] makes $\mathbf{x}_k$ a random variable, and consequently forecasts of the state dynamics must be in terms of some estimate of $\mathbf{x}_k$, such as the mean value. Additionally, it is desirable to quantify the distribution of x_k about that estimate, so that some type of confidence interval can be assigned.

Specifically, we seek an estimate $\hat{\mathbf{x}}_k \equiv [\hat{\overline{\theta}}_k, \hat{\overline{S}}_k]^T$ of $\mathbf{x}_k$ at future times, as well as the covariance of the estimation error, $\mathbf{P}_k = E[(\mathbf{x}_k - \hat{\mathbf{x}}_k)(\mathbf{x}_k - \hat{\mathbf{x}}_k)^T]$. Given an estimate of system state on day $k = 0$, $\hat{\mathbf{x}}_0 = \mathbf{x}_0$, and the error covariance, $\mathbf{P}_0$, it can be shown that the minimum mean square error estimate of $\mathbf{x}_k$ is given by (Gelb, 1974; Lewis, 1986)

$$\hat{\mathbf{x}}_{k+1} = \mathbf{a}(\hat{\mathbf{x}}_k) + \mathbf{B}\mathbf{u}_k. \quad [15]$$

The corresponding equation for the error covariance is (to first-order)

$$\mathbf{P}_{k+1} = \mathbf{A}_k\mathbf{P}_k\mathbf{A}_k^T + \mathbf{M}_k, \quad [16]$$

where

$$\mathbf{A}_k \equiv \left.\frac{d\mathbf{a}}{d\mathbf{x}}\right|_{x=\hat{x}_k}. \quad [17]$$

In these projection equations, it is assumed that $E[\mathbf{x}_0] = \hat{\mathbf{x}}_0$, $E[\mathbf{x}_0 - \hat{\mathbf{x}}_0)(\mathbf{x}_0 - \hat{\mathbf{x}}_0)^T] = \mathbf{P}_0$, and $\mathbf{w}_k = [w_k^\theta, w_k^s]^T$ is uncorrelated in time, zero mean Gaussian noise sequence with covariance $\mathbf{M}_k$.

Updating Forecasts When Measurements Are Available

Given daily measurements of the system forcing $\mathbf{u}_k$, Eq. [15] and [16] can be used to calculate $\hat{\mathbf{x}}_k$ and $\mathbf{P}_k$ in real time. Suppose at some time k we make a field measurement that provides information about system state $\mathbf{x}_k$. We would like to use this information to update our estimates of $\mathbf{x}_k$ and $\mathbf{P}_k$. To implement the filtering, we must specify the relationship between the measurements and the system state.

Measurement Equation

Rhoades et al. (1976) assumed that EC_b is comprised of a liquid phase conductivity and a solid phase conductivity (EC_s), and that the two conductivities can be modeled as parallel resistors. Noting that the liquid phase conductivity depends on the EC of the soil water (EC_w) as well as the transmission coefficient (T, a water content-dependent tortuosity factor), Rhoades et al. (1976) arrived at the following expression for the bulk soil EC:

$$EC_b = EC_w\theta T + EC_s, \quad [18]$$

where T is defined as

$$T = a\theta + b, \quad [19]$$

with empirical parameters a and b. Additionally, a common approximation is that EC_w is proportional to the total dissolved salt concentration (Marion and Babcock, 1976; U.S. Salinity Laboratory Staff, 1954),

$$C = KEC_w, \quad [20]$$

where the value of K is approximately 0.64 when EC is in dS m^{-1} and C is in mg mL^{-1} (Rhoades, 1986).

These relationships, along with the previously assumed $\overline{C}_k = \overline{S}_k/\overline{\theta}_k$, allow us to write an equation that relates the measurable quantities $\overline{\theta}_k$ and $\overline{EC}_{bk}$ to the state variables $\overline{\theta}_k$ and $\overline{S}_k$:

$$\begin{bmatrix}\overline{\theta}_k \\ \overline{EC}_{bk}\end{bmatrix} = \begin{bmatrix}\overline{\theta}_k \\ \overline{S}_k(a\overline{\theta}_k + b)/K + EC_S\end{bmatrix} + \begin{bmatrix}v_k^\theta \\ v_k^S\end{bmatrix}, \quad [21]$$

where $\mathbf{v}_k = [v_k^\theta, v_k^S,]^T$ is an error sequence (with variance $\mathbf{N}_k$) that accounts for errors in the measurement of $\overline{\theta}_k$ and $\overline{EC}_{bk}$,

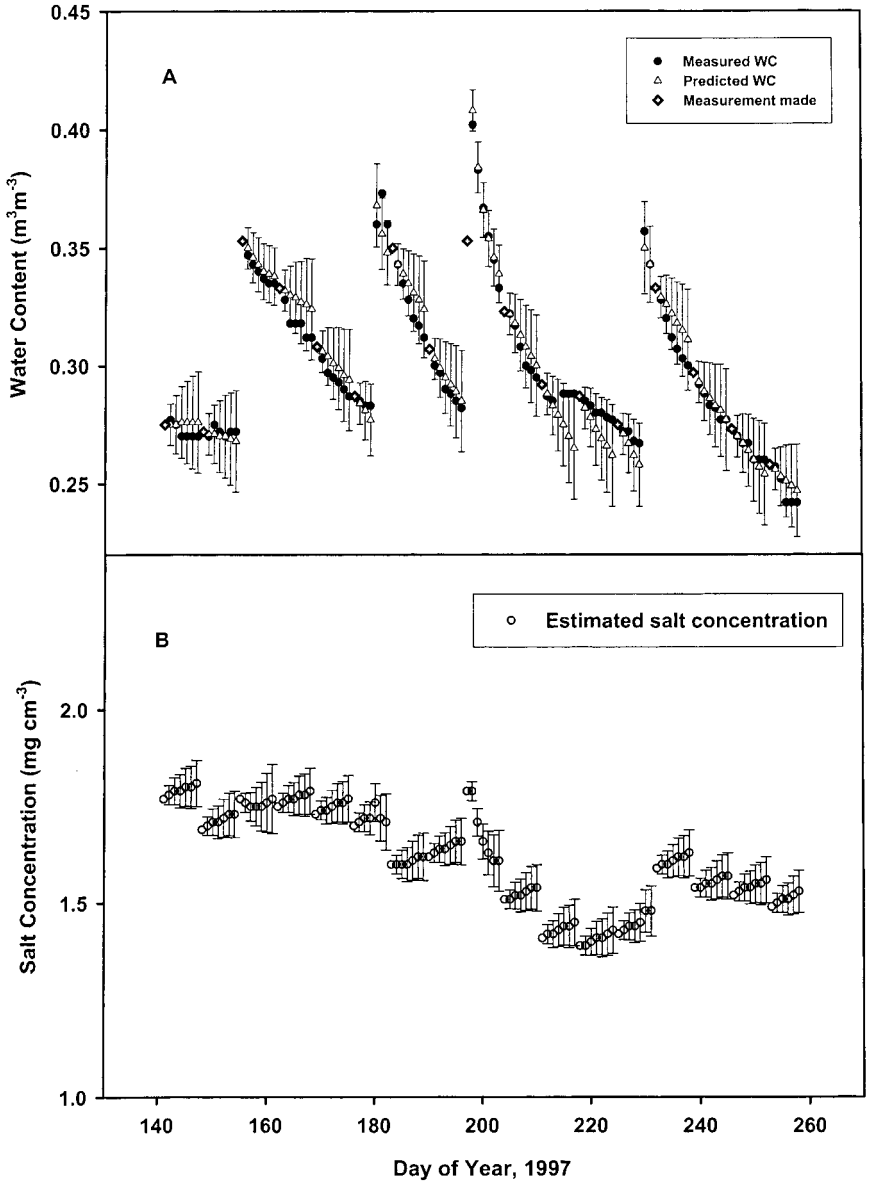

Fig. 3. (A) Time domain reflectometry measured and Kalman filter estimated profile-averaged soil water content (WC) and its estimation error and (B) Kalman filter estimated salt concentration (mg cm^{-3} soil) and its estimation error with weekly measurement update. The diamond symbol indicates the weekly water content measurement used to update the filter.

as well as uncertainties in the specified relationship between $\overline{EC}_{bk}$, $\overline{S}_k$, and $\overline{\theta}_k$.

Updating Forecasts with the Kalman Filter

The measurement Eq. [21] can be written more compactly as

$$\mathbf{z}_k = \mathbf{h}[\mathbf{x}_k] + \mathbf{v}_k \quad [22]$$

where $\mathbf{z}_k \equiv [\overline{\theta}_k, \overline{EC}_{bk}]^T$. If a measurement $\mathbf{z}_k$ is available and assuming $E[\mathbf{w}_j(\mathbf{v}_k)^T] = 0$, the projected state and error estimates are updated according to the extended KF (Gelb, 1974; Lewis, 1986)

$$\hat{\mathbf{x}}_k^+ = \hat{\mathbf{x}}_k^- + \mathbf{K}_k(\mathbf{z}_k - \mathbf{h}_k) \quad [23]$$

$$\mathbf{P}_k^+ = (\mathbf{I} - \mathbf{K}_k\mathbf{H}_k)\mathbf{P}_k^-(\mathbf{I} - \mathbf{K}_k\mathbf{H}_k)^T + \mathbf{K}_k\mathbf{N}_k\mathbf{K}_k^T \quad [24]$$

where superscripted pluses and minuses indicate updated and projected quantities, respectively, $\mathbf{I}$ is an identity matrix, and

$$\mathbf{K}_k = \mathbf{P}_k^-\mathbf{H}_k^T(\mathbf{H}_k\mathbf{P}_k^-\mathbf{H}_k^T + \mathbf{N}_k)^{-1}, \quad [25]$$

$$\mathbf{h}_k \equiv h[\hat{\mathbf{x}}_k^-], \quad [26]$$

$$\mathbf{H}_k \equiv \left.\frac{d\mathbf{h}}{d\mathbf{x}}\right|_{x=\hat{x}_k^-} \quad [27]$$

Parameter Estimation

The unknown parameters that need to be quantified are the noise covariances,

$$\mathbf{M}_k = \begin{bmatrix} M_k^\theta & 0 \\ 0 & M_k^S \end{bmatrix} \quad [28]$$

and

$$\mathbf{N}_k = \begin{bmatrix} N_k^\theta & 0 \\ 0 & N_k^S \end{bmatrix} \quad [29]$$

as well as the Rhoades et al. (1976) model parameters, a, b, and EC_s.

First, we assume that N_k^θ and N_k^S are zero, implying that the measurements of $\overline{\theta}_k$ and $\overline{EC}_{bk}$ are exact. This seems to be a reasonable first approximation given that our measurements are likely to be much more accurate than our simulation equations, which contain numerous simplifications and approximations. Specifying zero measurement error means that the state update Eq. [23] sets the estimate of the current system state to be equal to the value indicated by the measurement, and the error update Eq. [24] sets the estimation error to zero. Of interest, then, is how long we can forecast the system state without the estimation error becoming unacceptably large. In other words, how far into the future can we project the system state before we need a new measurement to reset the simulation model?

Next we assume that $\mathbf{M}_k$ is constant ($M_k^\theta = M^\theta$ and $M_k^S = M^S$). The value of M^θ was set equal to the variance of the residuals in Fig. 2, divided by L^2. The result was $M^\theta = 7.7 \times 10^{-5}$. An examination of the residuals in Fig. 2 as a function of time indicated some short-range temporal correlation in the residuals from Site 1 but not for Sites 2 and 3. The KF equations require $\mathbf{w}_k$ to be uncorrelated in time. We assume the small temporal correlations in the Site 1 data are insignificant when combined with data from all three sites (as we did in Fig. 2). M^S was subsequently determined by maximizing the likelihood function (Bras and Rodriquez-Iturbe, 1985):

$$\Phi(M^S) = -nm \ln(2\pi) - \sum_{k=1}^{n} \ln|\mathbf{N}_k + \mathbf{H}_k\mathbf{P}_k^-\mathbf{H}_k^T| - \sum_{k=1}^{n} (\mathbf{z}_k - \mathbf{h}_k)^T (\mathbf{N}_k + \mathbf{H}_k\mathbf{P}_k^-\mathbf{H}_k^T)^{-1} (\mathbf{z}_k - \mathbf{h}_k) \quad [30]$$

where $m = 2$ is the number of state variables and n is the number of measurements used in the fitting. We used the first $n = 60$ d of measurements from Site 1 for the fitting, and the fitted value was $M^S = 6 \times 10^{-4}$ mg^2 cm^{-2}.

Lastly, we use transmission coefficient parameters $a = 1.38$ and $b = -0.09$ (Rhoades et al., 1976) and assume the conductivity of the solid phase is negligibly small ($EC_s = 0$).

RESULTS AND DISCUSSION

We now consider the measured data in Fig. 1 more carefully. The profile-averaged water content increased during irrigation and decreased between irrigations due to drainage and ET. The apparent rate of water depletion from the soil profile decreased as time progressed in an irrigation cycle, presumably due to increased resistance to root water uptake and surface evapotranspiration from dry soil. Records maintained by the water district indicate that the field was irrigated during Days 208 through 216, with the irrigation volume being roughly two-thirds that applied during the previous irrigation (which encompassed Days 196–197). However, our three sites, which were located at the tail end of the field, apparently received only minimal amounts of water, if any, because the only increase in the total profile stored during this time was a slight increase of about 1 cm near Day 215. However, the water content in the surface layers (10 and 30 cm) did not increase on this day. Rather, the small increase was due to increasing water contents at the 90- and 110-cm depths. Because the surface layers did not show an increased water content, we decided for modeling purposes to assume that no irrigation occurred during this time (recall we calculated I_k based on measured changes in total water storage, Fig. 1C). As will be seen, this will have implications for our modeling results.

The EC_b data (Fig. 1B) mirrored the water content data, increasing during irrigation and decreasing during soil drying, indicating that EC_b is affected by the water content of the soil as well as the salinity of the soil. Equation [18] assumes that the water content component of EC_b can be separated from the salinity component giving us a measurement of soil solution electrical conductivity (EC_w).

Figure 3A compares the measured profile-averaged water content with $\overline{\theta}_k$, as calculated by Eq. [15] and [23] (the KF). The calculations were done assuming that a water content measurement was made every 7 d (weekly). These measurements are shown as open diamonds in Fig. 3A. Because we updated the forecast at these points (using Eq. [23]), the modeled and measured water contents coincide on these days and the error bars are zero (recall we have assumed zero measurement error). The other water content data shown in the figure are not used in the calculations and are shown only for comparison purposes. The error bars on the predicted water contents are equal to $\pm \sqrt{P_{11k}}$, where

$$\mathbf{P}_k = \begin{bmatrix} P_{11k} & P_{12k} \\ P_{21k} & P_{22k} \end{bmatrix}, \quad [31]$$

and $\mathbf{P}_k$ is calculated by Eq. [16] and [24]. As expected, the estimation error increases as the forecast gets further away from a measurement update.

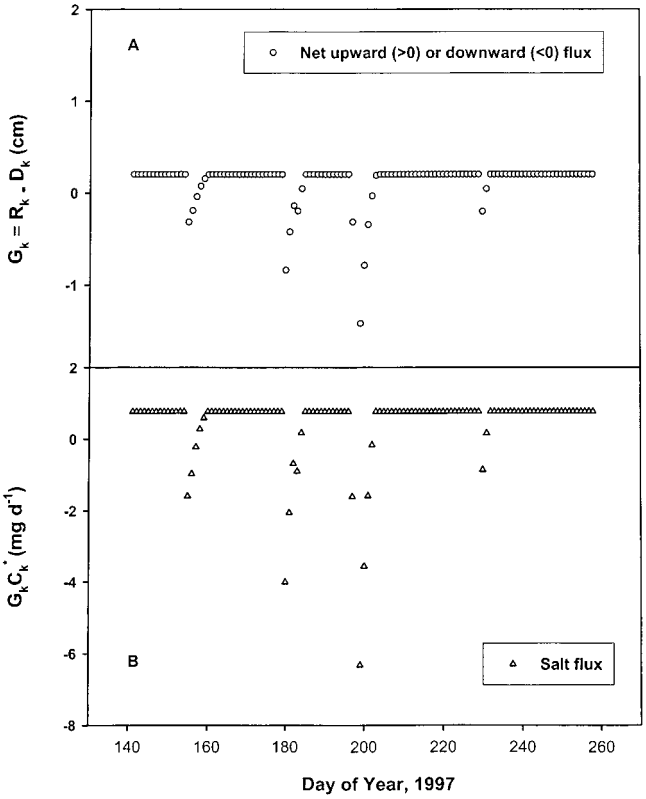

Fig. 4. Estimated (A) daily groundwater flux and (B) salt flux.

In general, the predicted values are close to the measured values, with the measured values falling within the predicted confidence intervals. The poorest results are found on Days 215 through 225, where relatively large differences between measured and predicted values are observed. The poor performance during this time period is partly, but not entirely, due to the ambiguous irrigation data that were discussed above. Poor performance is also seen after approximately Day 219, where the forecast water content decreases more rapidly than the measured water content. This discrepancy may be due to an overestimation of ET_a and/or an underestimation of the rate of upward groundwater flow by Eq. [9]. Nevertheless, the maximum difference between the forecast and measured water content during the period of relatively poor performance is only 0.023 ($m^3\ m^{-3}$), comparing the water content range of 0.24 to 0.41 in the field.

Figure 3B shows the profile-averaged resident salt concentration, $\overline{S}_k$ (mg cm^{-3} soil), as calculated by the KF equations. The timing of the measurement updating is the same as in Fig. 3A. The concentration changes in response to the loss of salt by leaching and the addition of salt by irrigation and upward groundwater flow. Although there are no measurements shown on the Fig. 3B, we can infer that the model is not tracking the data very well. Note that over much of the figure the model forecast between measurements shows an increasing salt concentration, whereas the trend of the measurement updates is decreasing or constant, leading to the sawtooth appearance of portions of the plot. The higher salt loading predicted by the model may be due to an overestimation of either the groundwater salt concentration or the rate of upward groundwater flow. Figure 4A shows the daily water flux, G_k at the bottom of the root zone, as computed in the KF calculations. Figure 4B shows the corresponding computed daily salt flux, $G_k C_k^*$.

Simultaneous with our forecasting and updating of $\overline{\theta}_k$ and $\overline{S}_k$, we can estimate EC_w *as*

$$\overline{EC_{wk}} = \frac{\overline{S}_k}{K\overline{\theta}_k} \quad [32]$$

This estimate of EC_w is shown in Fig. 5, where $\overline{\theta}_k$ and $\overline{S}_k$ are the KF calculations shown in Fig. 3 (weekly measurement updates). Also shown is the measured value of EC_w, which is given by (see Eq. [18])

$$\overline{EC_{wk}} = \frac{\overline{EC_{bk}} - EC_s}{\overline{\theta}_k(a\overline{\theta}_k + b)} \quad [33]$$

where $\overline{\theta}_k$ and $\overline{EC}_{bk}$ are the daily TDR measurements. As expected, the general trend is that EC_w increases as water is extracted by plant roots (increasing the soil water salt concentration) and decreases during irrigation (the salt concentration is diluted). Overall, there is good agreement between the daily measured values and the weekly forecast values, with the maximum difference being less than 1 dS m^{-1}.

Similarly, an estimate of EC_e is given by (see Rhoades, 1986, Eq. [10])

$$\overline{EC_{ek}} = \frac{\overline{S}_k}{K\rho_b SP/100}, \quad [34]$$

where SP = 62 is the soil saturation percentage and ρ_b = 1.29 g cm^{-3} is the soil bulk density. Figure 5 shows $\overline{EC}_{wk}$, where $\overline{S}_k$ is again the KF calculation from Fig. 3 that is based on weekly measurement updates. Figure 5 also shows the daily measured values (see Rhoades,

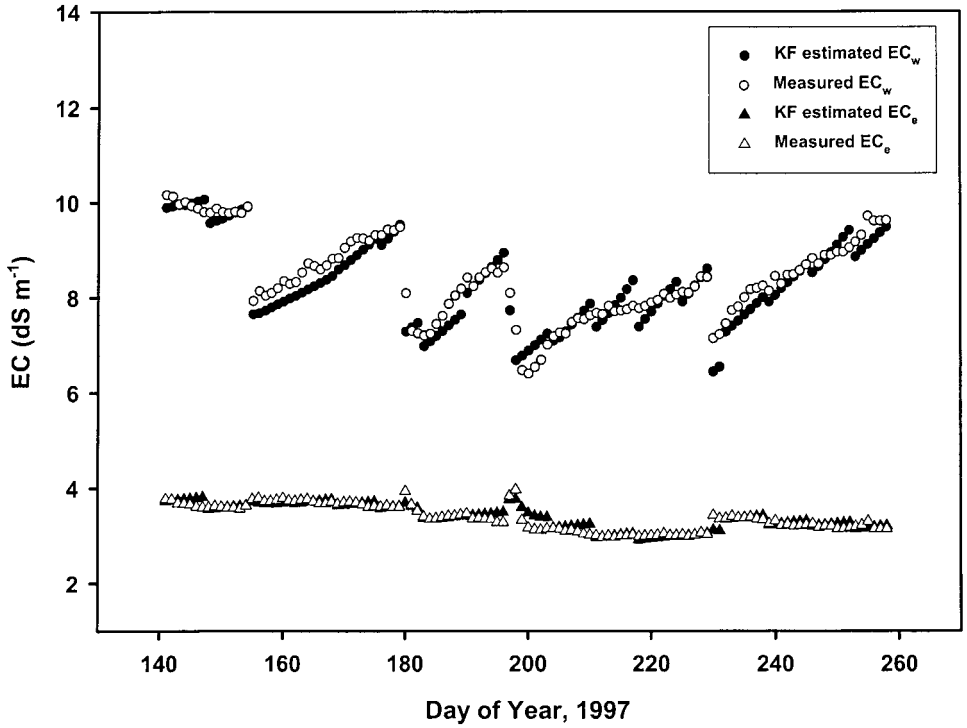

Fig. 5. Time domain reflectometry measured and Kalman filter (KF) estimated soil water electrical conductivity (EC_w) and electrical conductivity of saturated extract (EC_e) with weekly measurement update.

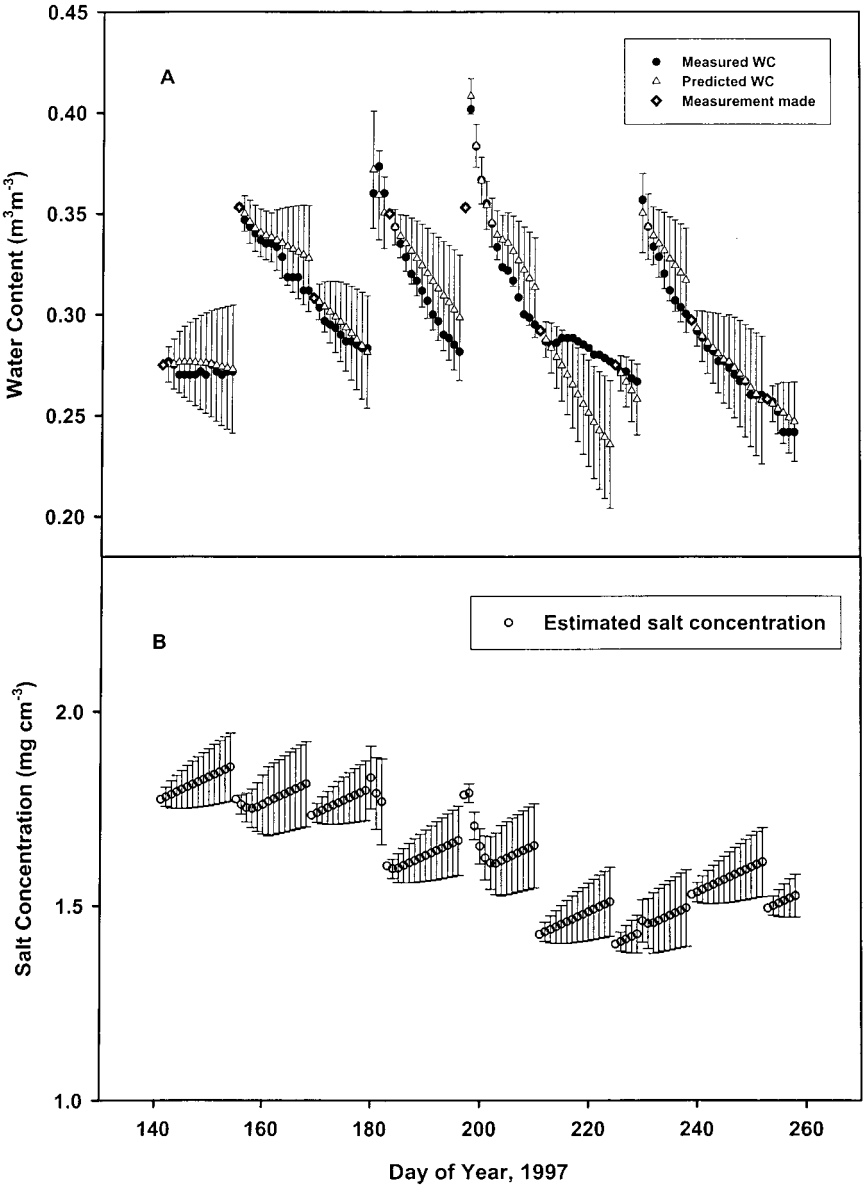

Fig. 6. (A) Time domain reflectometry measured and Kalman filter estimated profile-averaged soil water content (WC) and its estimation error and (B) Kalman filter estimated salt concentration (mg cm^{-3} soil) and its estimation error with biweekly measurement update. The diamond symbol indicates the biweekly water content measurement used to update the filter.

1986, Eq. [10]),

$$\overline{EC}_{ek} = \frac{\overline{EC}_{wk}\,\overline{\theta}_k}{\rho_b SP/100}. \qquad [35]$$

where $\overline{EC}_{wk}$ is given by Eq. [33] and $\overline{\theta}_k$ is the daily TDR measurement. The modeled and measured $\overline{EC}_{ek}$ are in good agreement. EC_e is the measure of root zone salinity that is used by agronomists, extension experts, and farmers to quantify the effects of salt on crop growth. Figure 5 shows that EC_e was essentially constant, indicating that the irrigation and shallow groundwater management practices used at the experimental site did not increase soil salinity during the 1997 growing season. No reductions in cotton yield would be expected with an average root-zone EC_e of 3.6 to 4 dS m^{-1}, and none were observed. The measured EC of a saturation extract made from a soil sample taken near Site 1 was EC_e = 3.6 dS m^{-1}, which is in good agreement with values shown in Fig. 5.

Figure 6 is directly analogous to Fig. 3 except the model forecasts now span 2 wk and the measurement updates are biweekly. The 2-wk interval coincides roughly with the irrigation cycle used by the farmer. The error bars continue to grow over the course of the 2-wk forecasts. The measured water contents fall within the prediction error bars, except for Days 215 through 225. Following the measurement update at Day 225, the modeled water content tracks the measured water content fairly well. The modeled resident salt concentrations in Fig. 3 and 6 show the same general trend, with the plot again exhibiting something of a sawtooth appearance. The computed water and salt fluxes were very similar to those in Fig. 4 and are not shown. Figure 7 shows the estimated and measured EC_w and EC_e using

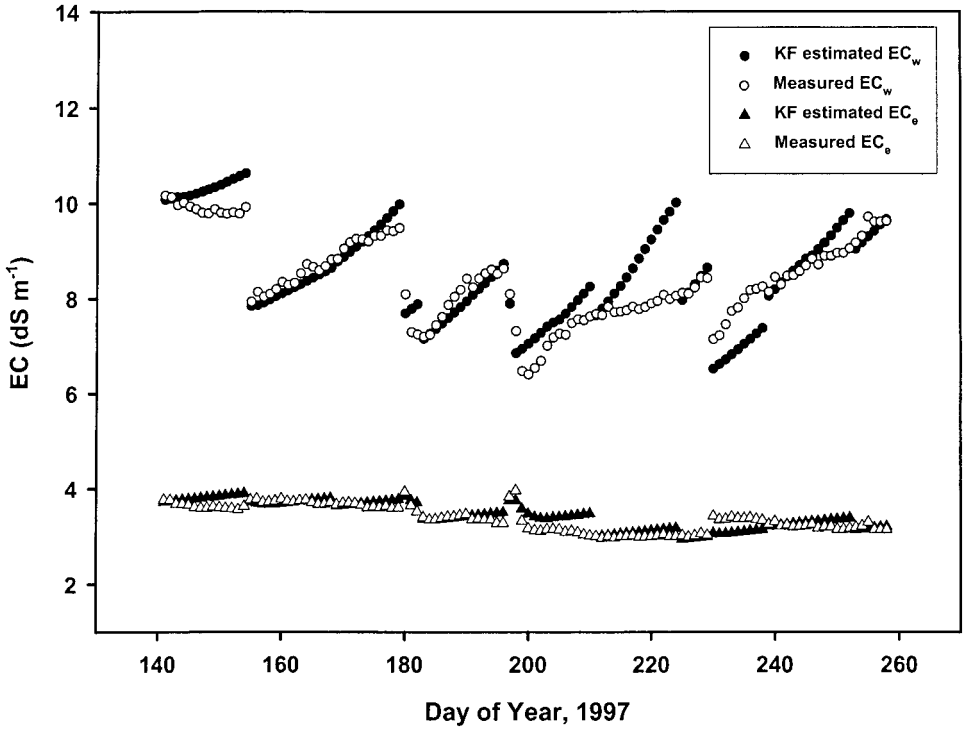

Fig. 7. Time domain reflectometry measured and Kalman filter (KF) estimated soil water electrical conductivity (EC_w) and electrical conductivity of saturated extract (EC_e) with biweekly measurement update.

the biweekly measurement updates. The results are similar to those seen in Fig 5. Overall, the modeled water and salinity dynamics were not substantially different for the 1- or 2-wk update interval.

SUMMARY AND CONCLUSIONS

In this study, a state-space model for profile-averaged water content and salt concentration were developed based on mass balance and an empirical relationship that specifies the water flux at the bottom of the root zone as a function of the profile-averaged water content. The water balance equation considers irrigation, precipitation, evapotranspiration, and root-zone drainage to and recharge from shallow groundwater. The salt balance equation considers dissolved salts in irrigation water, soil water, and groundwater. Based on our model, forecasts of state variables (profile-averaged water and salt contents) and the estimation error covariances at future times were obtained using daily ET and irrigation data as inputs. The forecasts were updated by Kalman filtering when measurements of soil water content and electrical conductivity were made available. We found that weekly and biweekly measurement updating could predict profile-averaged water content and EC_w reasonably well for the 1997 cotton growing season. A biweekly scheme is more in line with current irrigation practices for cotton on the west side of the San Joaquin Valley, California. A discrepancy between observed and forecast salt and water regimes during Days 215 to 225 was attributed to the net groundwater recharge–discharge not being accurately described by our assumed empirical relationship, and due to inaccurate irrigation data. The EC_e did not vary substantially during our study, so further testing of the proposed salinity dynamics model is warranted.

The forecast increases in EC_w seem to be realistic especially when EC_e is relatively constant throughout the season. Under our field conditions EC_e changed very slowly and EC_w could be estimated from Eq. [35] by the use of water content information. Thus, forecasting of both soil water content and EC_w could be done with periodic measurements of soil water content, and one single measurement of soil EC_e. In situations where soil water salinity above some threshold is detrimental to crop production, EC_w forecasts could be used to schedule irrigation timing and/or amount to alleviate salinity stress. Such an approach could be especially beneficial for high cash value crops that exhibit a high sensitivity to soil water salinity. Forecast of field soil water and salinity regimes can provide irrigation managers flexibility in irrigation scheduling and help prevent yield decline due to water and/or salinity stresses.

REFERENCES

Aboitiz, M., J. Labadie, and D. Heermann. 1986. Stochastic soil moisture estimation and forecasting for irrigated fields. Water Resour. Res. 22:180–190.

Ayars, J.E., and R.A. Schoneman. 1986. Use of saline water from shallow water table by cotton. Trans. ASAE 29:1674–1678.

Bras, R.L., and I. Rodríquez-Iturbe. 1985. Random functions and hydrology. Adison-Wesley, Reading, MA.

Gelb, A. (ed.) 1974. Applied optimal estimation. M.I.T. Press, Cambridge, MA.

Hipel, K.W., A.I. McLeod, and W.C. Lennox. 1977. Advances in Box-Jenkins modeling: 1. Model construction. Water Resour. Res. 13: 567–576.

Herkelrath, W.N., S.P. Hamburg, and F. Murphy. 1991. Automatic, real-time monitoring of soil moisture in a remote field area with time domain reflectometry. Water Resour. Res. 27:857–864.

Lewis, F.L. 1986. Optimal estimation. John Wiley & Sons, New York.
Marion, G.M., and K.L. Babcock. 1976. Predicting specific conductance and salt concentration in dilute aqueous [soil] solutions. Soil Sci. 122:181–187.
Or, D., and R.J. Hanks. 1992, Spatial and temporal soil water estimation considering soil spatial variability and evapotranspiration uncertainty. Water Resour. Res. 28:803–814.
Parlange, M.B., G.G. Katul, R.H. Cuenca, M.L. Kavvas, D.R. Nielsen, and M. Mata. 1992. Physical basis for a time series model of soil water content. Water Resour. Res. 28:2437–2446.
Rhoades, J.D. 1986. Soluble salts. p. 167–179. *In* A. Klute (ed.) Methods of soil analysis: Part 2. Chemical and microbiological properties. Agron. Monogr. 9. 2nd ed. ASA and SSSA, Madison, WI.
Rhoades, J.D., P. Raats, and R.J. Prather. 1976. Effects of liquid-phase electrical conductivity, water content, and surface conductivity on bulk soil electrical conductivity. Soil Sci. Soc. Am. J. 40:651–655.
Schaap, M.G., L. de Lange, and T.J. Heimovaara. 1996. TDR calibration of organic forest floor media. Soil Tech. 11:205–217.
Skaggs, T.H., and B.P. Mohanty. 1998. Water table dynamics in tile-drained fields. Soil Sci. Soc. Am. J. 62:1191–1196.
Torres, J.S., and R.J. Hanks. 1989. Modeling water table contribution to crop evapotranspiration. Irrig. Sci. 10:265–279.
University of California-Division of Agriculture and Natural Resources. 1996. Cotton production manual. Univ. of California.1996. Publ. 3352. Oakland, CA.
U.S. Salinity Laboratory Staff. 1954. Diagnosis and improvement of saline and alkali soils. USDA Agric. Handb. 60. USDA, Riverside, CA.
Wallender, W.W., D.W. Grimes, D.W. Henderson, and L.K. Stromberg. 1979. Estimating the contribution of a perched water table to the seasonal evapotranspiration of cotton. Agron. J. 71:1056–1060.
Whalley, W.R. 1993. Considerations on the use of time-domain reflectometry (TDR) for measuring soil water content. J. Soil Sci. 44:1–9.
Wu, L., W.A. Jury, and A.C. Chang. 1997. Time-series analysis of field-measured soil water content of a sandy soil. Soil Sci. Soc. Am. J. 61:736–742.

Predicting Temperature and Heat Flow in a Sandy Soil by Electrical Modeling

Dardo O. Guaraglia, Jorge L. Pousa,* and Leonardo Pilan

ABSTRACT

A model based on an electrical analogy between a soil column and an electrical transmission line was developed to predict temperature and heat flow as functions of depth and time in a sandy soil, taking into account changes in soil thermal conductivity and volumetric heat capacity due to variations in water content. The model was excited alternatively by both measured soil temperature at the 1-cm depth and solar radiation [$S_r(t)$], and solved with available electrical analysis software. The results were compared with field data collected during a 35-d field experiment carried out in the Lido beach, Venice, Italy. A very simple transfer function was identified for using measured $S_r(t)$ as the input signal. This transfer function turned out to vary inversely with $S_r(t)$. When the model is excited by temperature, and soil water content corrected every 5 d, the root mean square error (RMSE) for the calculated temperature at the 5-cm depth is less than 1°C. When it is excited by $S_r(t)$, the RMSE at the 1-cm depth is less than 2°C. Hourly temperatures at different depths were found to depend strongly on surface phenomena, and to a lesser extent on other factors like soil water content below the top layers.

MANY PHYSICAL MODELS have been developed in connection with agricultural studies to predict soil temperature with depth and time. Some of them require measurements of soil temperature at or near the soil surface (Wierenga and de Wit, 1970; Hanks et al., 1971). Other models use soil and air temperatures normalized with respect to daily maximum and minimum, and averaged over a given period of time to obtain temperature curves for predicting purposes (Gupta et al., 1981, 1982, 1983, 1984), or are based on averaged or filtered air and soil temperature information (Persaud and Chang, 1983, 1984; Parton, 1984; Kemp et al., 1992). These models predict maximum, minimum, and daily mean soil temperatures rather well. However, calculation of mean values during normalizing or filtering processes results in loss of high frequency information. According to the Nyquist theorem (Schwartz and Shaw, 1975), at least two input samples per hour are needed to reproduce a bandlimited random hourly soil temperature. Thus, models identified from input/output filtered data are not able to recover high frequency information because this information was not taken into account in the system (model) identification process. It can be concluded that these models are valid for predicting low frequency soil temperature fluctuations, but they do not seem to be the most adequate ones for predicting hourly temperature variations. Pikul (1991) and Katul and Parlange (1993) use a surface energy balance approach for predicting hourly surface temperature. Both models require information on air temperature, relative humidity, wind speed, and net radiation, in addition to rainfall (Pikul, 1991) and soil heat flux (Katul and Parlange, 1993).

Persaud and Chang (1983, 1984) state that temperature changes in the soil profile are mainly due to the transference of heat energy produced at the soil surface from incident $S_r(t)$. Gupta et al. (1981) report that soil

Dardo O. Guaraglia, CONICET, Dep. de Hidráulica, Facultad de Ingeniería, UNLP, La Plata, Argentina. Jorge L. Pousa, CONICET, Lab. de Oceanografía Costera, Facultad de Ciencias Naturales y Museo, UNLP, Casilla de Correo 45, (1900) La Plata, Argentina. Leonardo Pilan, CNR, Istituto per lo Studio della Dinamica delle Grandi Masse, Venezia, Italia. Received 31 July 2000. *Corresponding author (dguaragl@volta.ing.unlp.edu.ar).

Published in Soil Sci. Soc. Am. J. 65:1074–1080 (2001).

Abbreviations: c, specific heat (J kg^{-1} °C^{-1}); C_e, electrical capacitance (F); C_t, heat capacity per unit area of a soil layer (J °C^{-1} m^{-2}); f, frequency (Hz); G, electrical conductance (Ω^{-1}); $G_T(t)$, function equivalent to an electrical conductance (W m^{-2} °C^{-1}); $I_1(t)$, heat flow at the surface and within the top centimeter of soil (W m^{-2}); $I_2(t)$, heat flow transmitted below the 1-cm depth (W m^{-2}); L, electrical inductance (H); R-C, ladder of resistances and capacitances for modeling soil below the 1-cm depth; r, correlation coefficient; R_e, electrical resistance (Ω); R_t, thermal resistance per unit area of a soil layer (°C m^2 W^{-1}); $R_T(t)$, time dependent transfer function for the surface and top centimeter of soil (W^{-1} m^2 °C); RMSE, root mean square error; $S_r(t)$, solar radiation (W m^{-2}); t, time (s); $T_1(t)$, soil temperature at depth of 1 cm (°C); Z, electrical impedance (Ω); ΔT, temperature difference across a soil layer (°C); Δz, thickness of a surface-parallel soil layer (m); θ, soil water content (m^3 m^{-3}); κ, thermal diffusivity (m^2 s^{-1}); λ, thermal conductivity (W m^{-1} °C^{-1}); ρ, density (kg m^{-3}); ρc, volumetric heat capacity (J m^{-3} °C^{-1}); Φ, heat flux density (W m^{-2}).